Invest Ophthalmol Vis Sci. Author manuscript; available in PMC 2014 March 09.

Published in final edited form as:
Invest Ophthalmol Vis Sci. 2008 November ; 49(11): 5136–5143. doi:10.1167/iovs.08-1849.

Amyloid-β Deposits Lead to Retinal Degeneration in a Mouse Model of Alzheimer Disease

Allison Ning[1], **Jing Cui**[1], **Eleanor To**[1], **Karen Hsiao Ashe**[2], and **Joanne Matsubara**[1]

[1]Department of Ophthalmology and Visual Sciences, University of British Columbia, Vancouver, BC, Canada

[2]Department of Neurology, University of Minnesota, Minneapolis, Minnesota

Abstract

Purpose—To compare the temporal and spatial expression patterns of amyloid precursor protein (APP), amyloid-β deposits, inflammatory chemokines, and apoptosis in the retina of a mouse model of Alzheimer disease (AD).

Methods—Retinas of transgenic mice harboring a mutant presenilin (PS1) and a mutant APP gene were processed for TUNEL and immunohistochemistry with antibodies against APP, amyloid-β, monocyte chemotactic protein (MCP)-1, and F4/80. Comparisons were made between age groups and between transgenic and wild-type congeners.

Results—The neuroretina demonstrated age-dependent increases in APP in the ganglion cells (RGCs) and in neurons of the inner nuclear layer (INL). Amyloid-β demonstrated significant age-dependent deposition in the nerve fiber layer (NFL). TUNEL-positive RGC increased in an age-dependent fashion and in transgenic compared with wild-type congeners. Concomitant overexpression of MCP-1 and intense immunoreactivity for F4/80 suggested that RGCs upregulate MCP-1 in response to amyloid-β. Activated microglia proliferated in response to MCP-1. In the outer retina, retinal pigment epithelium (RPE) demonstrated moderate age-dependent APP immunoreactivity, but nearby drusenlike deposits were not present. Amyloid-β was observed in the choriocapillaris of the older animals.

Conclusions—Amyloid-β deposits accumulate with age in the retina of a transgenic mouse model of AD. The amyloid-β loads are accompanied by increased immunoreactivity for MCP-1, F4/80, and TUNEL-positive profiles in the RGC layer. The results suggest that amyloid-β causes neurodegeneration in the retina of the doubly mutant transgenic mouse model of AD.

Alzheimer disease (AD) is the most common form of dementia among older people and is the seventh leading cause of death in the United States. Although the disease principally affects the central nervous system (CNS) and memory, cognition, and behavior, complaints of visual disturbances are not uncommon in AD.[1,2] Recent studies have demonstrated that problems with vision in AD may arise not only from cortical abnormalities, but also from retinal abnormalities. Several studies have demonstrated abnormalities in the optic nerve

Corresponding author: Joanne Matsubara, Department of Ophthalmology and Visual Sciences, University of British Columbia, Eye Care Centre, 2550 Willow Street, Vancouver, BC V5Z 3N9 Canada; jms@interchange.ubc.ca.

Disclosure: **A. Ning**, None; **J. Cui**, None; **E. To**, None; **K. Hsiao Ashe**, None; **J. Matsubara**, None

head, a reduction in the number of optic nerve fibers, and in the thickness of the parapapillary and macular retinal nerve fiber layers (RNFL).[3–7] In addition to these anatomic changes, there are changes in the pattern electroretinograms associated with AD.[8–10] Furthermore, retinal blood flow studies have demonstrated a significant narrowing of the retinal veins and decreased retinal blood flow.[6,11] Thus, although the retina is affected in AD, little is known of the cellular mechanisms underlying the loss of visual function. Earlier histologic studies showed that retinal ganglion cells undergo extensive neurodegeneration in AD.[12,13] Several proposed mechanisms have been suggested for the retinal neurodegeneration, including inflammatory events, amyloid misfolding, and amyloid angiopathy.[11] Using an established mouse model of AD that develops characteristic AD-like amyloid-β deposits in the brain because of the coexpression of a mutant human amyloid precursor protein (APP) and a mutant human PS1 transgene,[14–16] we sought to gain further understanding of the retinal abnormalities that may be associated with the overexpression of APP. The significant amyloid load in the CNS of this transgenic animal model makes it an ideal candidate for the present study, which addresses the role of amyloid-β in the eye. In this study, we characterized the temporal and spatial expression patterns of APP, amyloid-β deposits, inflammatory chemokines, and apoptosis in the retina of the double-mutant APP/PS1 transgenic mouse.

Materials and Methods

Mouse Strains

Two strains of the bitransgenic APP/PS1 mouse were studied (Table 1). Strain 1 develops characteristic AD-like amyloid-β deposits in the brain because of the coexpression of a mutant human APP and a mutant human PS1 transgene (Tg 2576 x Tg1).[14–17] Strain 2 was obtained commercially (4462; Jackson Laboratories; Bar Harbor, ME) and harbors a mutant human presenilin 1 (DeltaE9) and a chimeric mouse/human APP (AppSwe) gene.[18] All procedures on animals were performed in compliance with the ARVO Statement for the Use of Animals in Ophthalmic and Vision Research. The animal protocol was approved by the Animal Care Committee at the University of British Columbia and by the Institutional Animal Care and Use Committee (IACUC) at the University of Minnesota.

Animals were deeply anesthetized with pentobarbital sodium and killed at 7.8, 10.5, or 27 months of age. The tissues were fixed by intracardial perfusion by using a saline rinse followed by 4% paraformaldehyde in phosphate buffer (PB). The eyes were dissected and postfixed in buffered 4% paraformaldehyde. Fixed tissues from strain 1 were shipped on ice packs to University of British Columbia (Vancouver BC, Canada) by overnight courier. The eyes were washed extensively in phosphate-buffered saline (PBS) at pH 7.4. Whole globes were embedded in paraffin and oriented in the sagittal plane to obtain 5-μm sections through the axis defined by the pupil and optic nerve. Tissue sections were mounted onto glass slides and stored at room temperature.

APP and Amyloid-β Immunohistochemistry

Tissue sections from both strains were deparaffinized and rehydrated by standard procedures. Sections underwent antigen retrieval in 10 mM sodium citrate buffer and

microwave heating for 13 to 16 minutes. Tissue sections were then washed with PBS (pH 7.4), treated with 0.3% hydrogen peroxide to abolish endogenous peroxidase activity, and blocked for 15 minutes with 1% bovine serum in PBS. The tissue sections were then incubated for 32 minutes with mouse anti-APP A4 monoclonal antibody and washed three times for 5 minutes with PBS. For amyloid-β immunohistochemistry, the sections underwent antigen retrieval in formic acid at room temperature for 6 minutes and incubation in a humidified chamber at room temperature with monoclonal mouse antibody against amyloid-β for 3 hours. Sections processed for APP or amyloid-β immunohistochemistry underwent standard incubations in secondary antibodies followed by incubation in avidin biotin peroxidase complex (ABC Standard Elite; Vector Laboratories, Burlingame, CA) according to the manufacturer's protocol, and aminoethylcarbazole (AEC) or diaminobenzidine (DAB) chromogenic reactions (Table 2).

F4/80 and MCP-1 Immunohistochemistry

After deparaffinization and rehydration, sections of tissue underwent antigen retrieval for 3 minutes at room temperature with proteinase K diluted per the manufacturer's protocol (Sigma-Aldrich, St. Louis, MO). Tissue sections were then rinsed, treated with 0.3% hydrogen peroxide to abolish endogenous peroxidase activity, and blocked for 30 minutes at room temperature with 3% normal rabbit serum and 0.3% Triton X-100 (TX-100) in PBS. A primary antibody against F4/80 or against MCP-1 was used per Table 2. The sections were incubated at room temperature for 1 hour followed by an incubation overnight at 4°C in a humidified chamber. Next, the sections were rinsed in PBS for 5 minutes and incubated in biotinylated secondary antibodies, followed by avidin biotin peroxidase complex according to the manufacturer's protocol. Antibody binding was visualized by a glucose oxidase driven DAB reaction resulting in a brown-black reaction product at sites of antibody binding.

All immunohistochemical sections were rinsed, counterstained with Mayer's modified hematoxylin, dehydrated, and coverslipped for light microscopy. Negative control sections were processed identically, but with the omission of the primary antibody. Immunohistochemistry on human brain tissue from a donor with Alzheimer disease served as a positive control for procedures using antibodies against APP and amyloid-β.

TUNEL Assay

After standard deparaffinization and rehydration procedures, tissue sections were subjected to antigen retrieval by heat retrieval with sodium citrate buffer (pH 6) and microwave heating. TUNEL solutions were prepared according to the manufacturer's protocol (Roche Diagnostics, Indianapolis IN). Briefly, the slides were rinsed in PBS and excess solution removed. Next, 25 μL of TUNEL reaction mixture was placed on each section and allowed to incubate in a humidified, darkened chamber for 1 hour at 37°C. The slides were then rinsed three times in PBS, counterstained with 4′, 6-diamidino-2-phenylindole (DAPI), and coverslipped with aqueous mounting medium (50% glycerol and 50% PBS). The sections were imaged on a confocal laser scanning microscope (LSM 510 META; Carl Zeiss Meditec, Dublin, CA). Other sections were processed for TUNEL with an alkaline phosphatase (AP) reaction that resulted in a blue-black reaction product (Figs. 1M, 1N). The sections were immersed with 25 μL of converter-AP solution and placed in a darkened,

humidified chamber for 30 minutes at 37°C. After the sections were rinsed three times in PBS, a nitroblue tetrazolium chloride/5-bromo-4-chloro-3-indolyl phosphate toluidine solution (NBT/BCIP; Roche Diagnostics) was placed on each section for 10 minutes at room temperature in a darkened chamber. The sections were then coverslipped with aqueous mounting medium (50% glycerol and 50% PBS) for bright-field microscopy.

Data Analysis

Cell profiles surrounded by F4/80-immunoreactive microglia in the GCL were quantified. Semiquantitative analysis was conducted by examination of five fields per tissue section, using a 40× objective lens and 10× eyepieces in a masked fashion. The number of cell profiles in the GCL surrounded by positively labeled F4/80 microglia was identified, and a percentage was calculated from the total number of retinal ganglion cells in each section. Between four and five tissue sections per eye and two eyes from each age group (strain 1) and from transgenic and wild-type congeners (strain 2) were analyzed.

TUNEL staining was analyzed by counting all the TUNEL-positive cell profiles in the GCL in each section. The value was then divided by the linear length of retina analyzed to obtain an average number of TUNEL-positive profiles per 100 μm of GCL. The average was obtained from two animals in each age group (strain 1) or in the transgenic and wild-type congener groups (strain 2).

A Student's *t*-test (unequal variance) was used for statistical analyses of immunohistochemical and TUNEL data from the two age groups or between transgenic and wild-type congener groups. A one-tailed test was selected based on the directional hypothesis that F4/80 immunoreactivity and TUNEL-positive profiles would be greater in the 27-month-old (compared with the 7.8-month-old) or in the transgenic (compared to the wild-type) animals. The significance level was set at $P < 0.05$.

Results

Strain 1

APP immunoreactivity was present in the cytoplasmic compartment of cell profiles in the GCL and inner nuclear layer (INL) of the retinas in transgenic animals of both age groups. The intensity of cellular labeling was significantly stronger and more robust in the retinas of the 27-month-old (Fig. 1A) than in the 7.8-month-old (Fig. 1B) animals. The neuropil in the inner (IPL) and outer (OPL) plexiform layers and the photoreceptor outer segments (OS) were strongly immunoreactive in the 27-month-old animals (Fig. 1A). Neurons in the outer nuclear layer (ONL) did not display APP immunoreactivity in either age group (Figs. 1A, 1B).

The RPE in the outer retina was moderately immunoreactive for APP in the 27-month-old animals, whereas the RPE of the 7.8-month-old eyes displayed only background (nonspecific) levels of immunoreactivity (Figs. 1C, 1D).

Immunoreactivity for extracellular deposits of amyloid-β was robust in the inner retina, principally on the NFL and surrounding the cell profiles in the GCL in the 27-month-old

eyes (Fig. 1E and inset). In contrast, amyloid-β immunoreactivity was virtually absent from the retinal tissues of the 7.8-month-old animals (Fig. 1F). Amyloid-β deposits were also seen in the microvasculature, both in the retina (Fig. 1E, arrowheads) and choriocapillaris (Fig. 1G, arrows) of the 27-month-old animals only.

Immunoreactivity for F4/80 demonstrated microglial populations surrounding cell profiles in the GCL and sporadic microglial populations in the IPL and the OPL of the 27-month-old retinas (Fig. 1I, arrowhead). The 7.8-month-old retinas displayed less immunoreactivity in the GCL. Sporadic microglial profiles were evident in the OPL in this age group. The number of cell profiles in the GCL that were surrounded by F4/80-immunoreactive microglia was significantly greater in the 27-month-old retinas. The average percentage of cells in the GCL surrounded by F4/80-immunoreactive microglial cells was 50% (SD = 15.9%) in the 27-month-old and 10% (SD = 4.2%) in the 7.8-month-old groups and reached significance ($P < 0.05$; Fig. 2A). Other cell types of the retina were not surrounded by F4/80-immunoreactive microglia.

Immunoreactivity for MCP-1 was present in the cytoplasmic compartment of the cell profiles in the GCL of 27-month-old compared to 7.8-month-old retinas (Figs. 1K, 1L, and insets). Cells outside of the GCL were negative for MCP-1 immunoreactivity.

Apoptosis was studied by TUNEL labeling methods. With the TUNEL-AP method, only cell profiles in the GCL were TUNEL-positive (Figs. 1M, 1N, and insets). There was a significant increase in the number of TUNEL-positive profiles in the RGC layer of the 27-month-old compared with the 7.8-month-old animals (Fig. 2B; 1.42 cells/100 μm retina compared with 0.46 cells/100 μm retina; $P < 0.05$).

Strain 2

APP immunoreactivity was strongest in the cytoplasmic compartment of cell profiles in the GCL, a trend that was consistent with results from strain 1. However, unlike those in strain 1, cells in the INL and RPE layers did not display immunoreactivity for APP. The age-matched wild-type congeners did not display APP immunoreactivity in the RGC layer or any other layer of the retina (Figs. 3A, 3B).

Consistent with strain 1, amyloid-β immunoreactive deposits were present on the NFL and throughout the choroidal vasculature in strain 2. However, unlike in strain 1, the deposits were not found in the retinal vasculature in strain 2. Amyloid-β immunoreactivity was not evident in the age matched wild-type congener animals (Figs. 3C, 3D).

Immunoreactivity against F4/80 surrounded cells in the GCL at low levels in the strain 2 animals. F4/80 immunoreactivity was sporadically present in the IPL, but not evident in the OPL. Small F4/80-immunoreactive microglial profiles were evident in both transgenic and wild-type congeners (Figs. 3E, 3F).

Immunoreactivity for MCP-1 was present in the cytoplasmic compartment of the cell profiles in the GCL of transgenic retinas (Fig. 3G). Cells other than those in the GCL were negative for MCP-1 immunoreactivity. Wild-type congeners did not display MCP-1 immunoreactivity above background (Fig. 3H).

TUNEL-positive cells were seen in the GCL of both transgenic and wild-type congeners. There was a significant increase in the number of TUNEL-positive profiles in the GCL of the transgenic (1.6 cells/100 μm retina) compared to the age-matched wild-type control animals (1.0 cells/100 μm retina; Fig. 2C).

Discussion

Comparisons of Strains

We used two strains of APP/PS1 bitransgenic mice that have been studied previously for neurodegenerative, cognitive, and memory deficits associated with amyloid-β deposition in the CNS. Strain 1 bears a hamster prion promoter and a platelet derived growth factor (PDGF) promoter.[14–16] Strain 2 harbors a mouse prion promoter for both transgenes. The hamster prion, mouse prion, and the PDGF promoter are all known for their ability to target expression of transgenes specifically to neuronal cell types of the CNS.[18,19] Although some literature exists for retinal expression induced by the hamster prion promoter,[20] less is known about the activity of the mouse prion or PDGF promoters in the retina. Thus, it is possible that the differences observed in the immunohistochemical analyses between strain 1 and 2 shown here may be promoter-specific. As far as we know, this study is the first to provide results on gene overexpression associated with the mouse prion and PDGF promoters in the retina of transgenic mice.

Our characterization studies demonstrated many similarities among the two strains. Both strains demonstrated immunoreactivity against APP, principally in the cells of the GCL. In strain 1, there was a significant increase in APP expression in the 27-month-old animals, which is consistent with the previously characterized age-dependent overexpression of APP seen in the CNS.[14] A comparison between retinal tissue from transgenic and wild-type littermates in strain 2 revealed significant APP expression in the transgenic animals only. Amyloid-β immunoreactivity was observed principally overlying the NFL in both strains, and significantly robust immunoreactivity was evident in the 27-month-old animals of strain 1. Amyloid-β deposits were also seen in the retinal and choroidal vasculature of both strains, with robust immunoreactivity present in the 27-month-old animals of strain 1. Concomitant with the amyloid-β deposits, we observed an upregulation of MCP-1 by cells in the GCL in both strains. One main difference between the two strains was seen in the immunoreactivity for F4/80, a microglia marker in rodent retina. Strain 1 demonstrated an increased number of F4/80 microglia profiles surrounding cells in the GCL in the 27-month-old animals only. Strain 2 demonstrated F4/80 immunoreactivity in both the transgenic and wild-type congeners. The amyloid-β deposits as well as the MCP-1 immunoreactivity in strain 2 were of only moderate intensity and thus the lack of F4/80-immunoreactive profiles may represent the earliest stage of inflammation before microglial activation. As strain 2 animals, at 10.8 months of age, were intermediate between the old and young groups of strain 1, it is consistent that the levels of immunoreactivity in strain 2 were intermediate between the two age groups of strain 1.

Amyloid-β and Age-Related Retinal Changes

This study looked at the effects of APP overexpression and amyloid-β deposits in the retina of a mouse model of AD. Although the data are correlative, the immunohistochemical results suggest that the amyloid-β load in the retina of the 27-month animals in strain 1 promoted the overexpression of MCP-1 by cells in the GCL. Chemokines, such as MCP-1, are expressed by RGCs and attract macrophages and microglia in several retinal disorders.[21–23] As amyloid-β is a neurotoxic peptide, its presence in the NFL and GCL may also promote apoptosis, leading to the significant increase in TUNEL-positive cells in the GCL of the 27-month-old animals. Downstream effects of apoptotic pathways may result in the further activation of microglia populations to phagocytize and remove cellular debris associated with dead cells (Fig. 4).

Retinal abnormalities such as atrophy of the NFL, loss of cells in the GCL, and an increase in astrocyte glial cells in AD were first reported by Hinton et al.[12] and later confirmed by larger samples in follow-up studies by Blanks et al.[24,25] and are consistent with the findings reported herein. However, an important difference in the results obtained from clinical specimens and those reported here using a transgenic mouse model is that amyloid-β deposits have not yet been reported in the retinas of patients with AD.[24–26] It is possible that earlier histopathologic studies on the retinas of patients with AD missed amyloid-β deposits by using thioflavin S staining. Future studies involving more sensitive and specific methods may be useful in demonstrating amyloid deposits in postmortem retinal tissue from patients with AD. Alternatively, the observed retinal abnormalities and loss of visual function associated with AD may be due to decreased retinal blood flow[11] or from the sequelae of cerebral amyloid angiopathy, also known to arise in AD and suggested to underlie the pathogenesis of vision loss in these patients.[27–29] In the present study, retinal blood flow was not studied, but there is evidence of amyloid accumulation in the retinal and choroidal vasculature of the transgenic animals that may have affected local blood flow as well as cerebrovascular dysregulation in these animals.[29,30]

In this study, the retina of the bitransgenic mouse model of AD underwent an age-dependent increase in amyloid-β load, and a concomitant increase in expression of MCP-1 chemokine and microglial activation (Fig. 4). These processes may support apoptotic pathways within cells of the GCL in experimental AD.

Amyloid-β and Eye Disease

Retinal abnormalities in AD have been attributed to amyloidosis, with accumulation in the retinal vasculature as described earlier, or possibly in the retina itself. Recent studies have suggested that amyloid-β accumulation in the retina is also involved in the pathogenesis of two eye diseases: age-related macular degeneration (AMD) and glaucoma. AD, AMD, and glaucoma are all age-related neurodegenerative diseases. In AD, extracellular deposits of amyloid-β peptides in plaques and neurofibrillary tangles have been linked to neurodegeneration and inflammation in the brain.[31–33] In AMD, drusen deposits, the abnormal, extracellular deposits of cellular debris located between Bruch's membrane (BM) and the RPE, contain complement proteins and amyloid-β peptides.[34–37] It has been suggested that drusen deposits are the site of local chronic inflammation and that their

presence signals an altered patho-physiological state of the RPE.[33,34,38] Other studies have reported that specific polymorphisms in the human complement factor H (CFH) gene increase the risk of AMD by several fold.[39–43] It is still not known what triggers the complement cascade in AMD; however, amyloid-β may be a candidate peptide, as it has a known role in promoting the complement pathways in AD.[44,45] Neurodegenerative events have also been linked to amyloid-β in both AD and AMD. In AMD, a recent postmortem study reported that photoreceptors adjacent to drusen sites exhibit abnormal synaptic morphology and neurodegeneration.[46] Future studies should address whether amyloid-β alone, or in concert with complement proteins,[47] oxidatively modified proteins[48] and/or whether amyloid oligomers[49] contribute to synaptic disease and retinal degeneration, as all are constituents of drusen. Recently, amyloid-β immunotherapy improved ERG deficits and decreased amyloid deposits in the eye and brain of a mouse model of AMD, suggesting that amyloid-β immunotherapy attenuates and slows the progression of AMD.[50]

In this study, surprisingly, few degenerative changes were observed in the outer retina of the 27-month-old-old APP/PS1 bitransgenic mouse. Whereas RPE cells demonstrated a moderate age-dependent overexpression of APP, there were no amyloid-β deposits, or drusen-like profiles, surrounding the RPE and BM. There was, however, evidence of moderate amyloid-β deposits in the microvasculature of the choroidal circulation underlying the BM in 27-month-old eyes. One possible explanation for the observed differences between the neurons of the inner retina and the RPE of the outer retina is the cellular specificity of the promoter used in the animal models we studied. It is possible that the prion promoter favored expression in neuronal more than in RPE cell populations. Future studies using a promoter such as one from the tyrosine kinase family[51] may allow us to understand the downstream events associated with overexpression of APP by the RPE and whether this may cause an accumulation of amyloid-β or drusen-like deposits in the outer retina.

Amyloid-β deposition in the retina has also been implicated in glaucoma. To the best of our knowledge, there have not been any reported cases of amyloid-β accumulation in glaucomatous donor eyes obtained postmortem. However, two recent studies demonstrated that abnormal tau (AT8)[52] and phosphorylated tau (Tseng H, et al. *IOVS* 2007;48:ARVO E-Abstract 3269) are present in human ocular tissues of patients with uncontrolled intraocular pressure and in donor eyes with glaucoma. Much stronger evidence for amyloid-β's role in glaucoma exists from studies of experimental glaucoma in which several animal models were used. It was shown earlier that APP and amyloid-β are present in the retinal ganglion cells after elevated intraocular pressures (IOP) in a rat model[53,54] and in the DBA/2J spontaneous mouse model of long-lasting, chronic ocular hypertension.[55] MacKinnon et al. [53] have shown that in response to chronic elevated IOP, ganglion cells undergo changes that promote caspase activation and abnormal processing of APP. These changes in experimental glaucoma in response to chronic elevated IOP may contribute to the neurodegenerative events associated with the pathophysiology of glaucoma. Similarly, Goldblum et al.[55] demonstrated that strong APP and amyloid-β immunoreactivity is associated with the GCL and optic nerve of old DBA/2J mice. Recently, Guo et al.[56] demonstrated that the inhibition of the formation of amyloid-β at different sites of the pathway can minimize ganglion cell apoptosis in a rodent model of unilateral elevated IOP induced by hypertonic saline injection in the episcleral veins. These studies suggest potential avenues for future work focused on

understanding the relationship between amyloid-β and neurodegeneration in both experimental and human glaucoma.

In summary, the APP/PS1 mouse model of AD studied herein demonstrate significant age-related amyloid-β load overlying the NFL and in the retinal and choroidal vasculature. Concomitant age-related increases in the inflammatory cytokine, MCP-1, and microglia marker, F4/80, as well as apoptotic profiles in the cells of the GCL suggest that amyloid-β plays a significant role in the inflammation and neurodegeneration in the retina in experimental AD. Animal models of AD may be useful in elucidating the role of amyloid-β in retinal neurodegeneration.

Acknowledgments

Supported by the Canadian Institutes of Health Research (CIHR) and the Helen Keller Foundation (JM).

The authors thank Weihong Song and Paul Fraser for contributing eye tissues from animals harboring a single mutation in APP, Stephanie Cheung for technical assistance, and Pat McGeer for contributing the sample of AD brain tissue used as the positive control tissue in this study.

References

1. Sadun AA, Borchert M, DeVita E, Hinton DR, Bassi CJ. Assessment of visual impairment in patients with Alzheimer's disease. Am J Ophthalmol. 1987; 104(2):113–120. [PubMed: 3618708]
2. Baker DR, Mendez MF, Townsend JC, Ilsen PF, Bright DC. Optometric management of patients with Alzheimer's disease. J Am Optom Assoc. 1997; 68(8):483–494. [PubMed: 9279048]
3. Tsai CS, Ritch R, Schwartz B, et al. Optic nerve head and nerve fiber layer in Alzheimer's disease. Arch Ophthalmol. 1991; 109(2):199–204. [PubMed: 1993028]
4. Hedges TR 3rd, Perez Galves R, Speigelman D, Barbas NR, Peli E, Yardley CJ. Retinal nerve fiber layer abnormalities in Alzheimer's disease. Acta Ophthalmol Scand. 1996; 74(3):271–275. [PubMed: 8828725]
5. Danesh-Meyer HV, Birch H, Ku JY-F, Carroll S, Gamble G. Reduction of optic nerve fibers in patients with Alzheimer disease identified by laser imaging. Neurology. 2006; 67:1852–1854. [PubMed: 17130422]
6. Iseri PK, Altinas O, Tokay T, Yuksel N. Relationship between cognitive impairment and retinal morphological and visual functional abnormalities in Alzheimer disease. J Neuroophthalmol. 2006; 26(1):18–24. [PubMed: 16518161]
7. Paquet C, Boissonnot M, Roger F, Dighiero P, Gil R, Hugon J. Abnormal retinal thickness in patients with mild cognitive impairment and Alzheimer's disease. Neurosci Lett. 2007; 420(2):97–99. [PubMed: 17543991]
8. Trick GL, Barris MC, Bickler-Bluth M. Abnormal pattern electroretinograms in patients with senile dementia of the Alzheimer type. Ann Neurol. 1989; 26(2):226–231. [PubMed: 2774510]
9. Katz B, Rimmer S, Iragui V, Katzman R. Abnormal pattern electroretinogram in Alzheimer's disease: evidence for retinal ganglion cell degeneration? Ann Neurol. 1989; 26(2):221–225. [PubMed: 2774509]
10. Parisi V, Restuccia R, Fattapposta F, Mina C, Bucci MG, Pierelli F. Morphological and functional retinal impairment in Alzheimer's disease patients. Clin Neurophysiol. 2001; 112(10):1860–1867. [PubMed: 11595144]
11. Berisha F, Feke GT, Trempe CL, McMeel JW, Schepens CL. Retinal abnormalities in early Alzheimer's disease. Invest Ophthalmol Vis Sci. 2007; 48(5):2285–2289. [PubMed: 17460292]
12. Hinton DR, Sadun AA, Blanks JC, Miller CA. Optic-nerve degeneration in Alzheimer's disease. N Engl J Med. 1986; 315(8):485–487. [PubMed: 3736630]
13. Blanks JC, Torigoe Y, Hinton DR, Blanks RH. Retinal degeneration in the macula of patients with Alzheimer's disease. Ann N Y Acad Sci. 1991; 640:44–46. [PubMed: 1776758]

14. Holcomb L, Gordon MN, McGowan E, et al. Accelerated Alzheimer-type phenotype in transgenic mice carrying both mutant amyloid precursor protein and presenilin 1 transgenes. Nat Med. 1998; 4(1):97–100. [PubMed: 9427614]
15. Hsiao K, Chapman P, Nilsen S, Eckman C, Harigaya Y, Younkin S. Correlative memory deficits, Abeta elevation, and amyloid plaques in transgenic mice. Science. 1996; 274:99–102. [PubMed: 8810256]
16. Duff K, Eckman C, Zehr C, et al. Increased amyloid-beta 42(43) in brains of mice expressing mutant presenilin 1. Nature. 1996; 383:710–713. [PubMed: 8878479]
17. Westerman MA, Cooper-Blacketer D, Mariash A, et al. The relationship between Abeta and memory in the Tg2576 mouse model of Alzheimer's disease. J Neurosci. 2002; 22(5):1858–1867. [PubMed: 11880515]
18. Jankowsky JL, Slunt HH, Ratovitski T, Jenkins NA, Copeland NG, Borchelt DR. Co-expression of multiple transgenes in mouse CNS: a comparison of strategies. Biomol Eng. 2001; 17(6):157–165. [PubMed: 11337275]
19. Games D, Adams D, Alessandrini R, et al. Alzheimer-type neuropathology in transgenic mice overexpressing V717F beta-amyloid precursor protein. Nature. 1995; 373(6514):523–527. [PubMed: 7845465]
20. Chishti MA, Strome R, Carlson GA, Westaway D. Syrian hamster prion protein (PrP) is expressed in photoreceptor cells of the adult retina. Neurosci Lett. 1997; 234:11–14. [PubMed: 9347934]
21. Yoshida S, Yoshida A, Ishibashi T, Elner SG, Elner VM. Role of MCP-1 and MIP-1 alpha in retinal neovascularization during post-ischemic inflammation in a mouse model of retinal neovascularization. J Leukoc Biol. 2003; 73:137–144. [PubMed: 12525571]
22. Ambati J, Anand A, Fernandez S, Sakurai W, Lynn BC, Kuziel WA. An animal model of age-related macular degeneration in senescent Ccl-2 or Ccr-2 deficient mice. Nat Med. 2003; 9:1390–1397. [PubMed: 14566334]
23. Davies MH, Eubanks JP, Powers MR. Microglia and macrophages are increased in response to ischemia-induced retinopathy in the mouse retina. Mol Vis. 2006; 12:467–477. [PubMed: 16710171]
24. Blanks JC, Torigoe Y, Hinton DR, Blanks RHI. Retinal pathology in Alzheimer's disease. I. Ganglion cell loss in foveal/parafoveal retina. Neurobiol Aging. 1996; 17:377–384. [PubMed: 8725899]
25. Blanks JC, Schmidt SY, Torigoe Y, Porrello KV, Hinton DR, Blanks RHI. Retinal pathology in Alzheimer's disease. II. Regional neuron loss and glial changes in GCL. Neurobiol Aging. 1996; 17:385–395. [PubMed: 8725900]
26. Curcio CA, Drucker DN. Retinal ganglion cells in Alzheimer's disease and aging. Ann Neurol. 1993; 33:248–257. [PubMed: 8498808]
27. Vinters HV, Wan ZZ, Secor DL. Brain parenchymal and microvascular amyloid in Alzheimer's disease. Brain Pathol. 1996; 6:179–195. [PubMed: 8737932]
28. Suo Z, Humphrey J, Kundz A, Sethi F. Soluble Alzheimer's beta amyloid constricts the cerebral vasculature in vivo. Neurosci Lett. 1998; 257:77–80. [PubMed: 9865931]
29. Fryer JD, Taylor JW, DeMattos RB, et al. Apolipoprotein E markedly facilitates age-dependent cerebral amyloid angiopathy and spontaneous hemorrhage in amyloid precursor protein transgenic mice. J Neurosci. 2003; 23:7889–7896. [PubMed: 12944519]
30. Niwa K, Younkin L, Ebeling C, Turner SK, Westaway D, Younkin S. AB1–40-related reduction in functional hyperemia in mouse neocortex during somatosensory activation. Proc Natl Acad Sci. 2000; 97:9735–9740. [PubMed: 10944232]
31. Wyss-Coray T. Inflammation in Alzheimer disease: driving force, bystander or beneficial response? Nat Med. 2006; 12:1005–1015. [PubMed: 16960575]
32. McGeer PL, McGeer EG. Local neuroinflammation and the progression of Alzheimer's disease. J Neurovirol. 2002; 8:529–538. [PubMed: 12476347]
33. Anderson DH, Talaga KC, Rivest AJ, Barron E, Hageman GS, Johnson LV. Characterization of β amyloid assemblies in drusen: the deposits associated with aging and age-related macular degeneration. Exp Eye Res. 2004; 78:243–256. [PubMed: 14729357]

34. Johnson LV, Leitner WP, Rivest AJ, Staples MK, Radeke MJ, Anderson DH. The Alzheimer's Aβ-peptide is deposited at sites of complement activation in pathologic deposits associated with aging and age-related macular degeneration. Proc Natl Acad Sci U S A. 2002; 99:11830–11835. [PubMed: 12189211]
35. Dentchev T, Milam AH, Lee VMY, Trojanowski JQ, Dunaief JL. Amyloid-β is found in drusen from some age-related macular degeneration retinas, but not in drusen from normal retinas. Mol Vis. 2003; 9:184–190. [PubMed: 12764254]
36. Green, RG., Harlan, JB. Histopathologic features. In: Berger, JW.Fine, SL., Maguire, MG., editors. Age-Related Macular Degeneration. St. Louis, MO: Mosby; 1999. p. 81-154.
37. Bressler SB, Maguire MG, Bressler NM, Fine SL. Relationship of drusen and abnormalities of the retinal pigment epithelium to the prognosis of neovascular macular degeneration. The Macular Photocoagulation Study Group. Arch Ophthalmol. 1990; 108:1442–1444. [PubMed: 1699513]
38. Seth A, Cui J, To E, Kwee M, Matsubara J. Complement associated deposits in the human retina. Invest Ophthalmol Vis Sci. 2008; 49(2):743–750. [PubMed: 18235023]
39. Klein RJ, Zeiss C, Chew EY, et al. Complement factor H polymorphism in age-related macular degeneration. Science. 2005; 308(5720):385–389. [PubMed: 15761122]
40. Edwards AO, Ritter R 3rd, Abel KJ, Manning A, Panhuysen C, Farrer LA. Complement factor H polymorphism and age-related macular degeneration. Science. 2005; 308:421–424. [PubMed: 15761121]
41. Hageman GS, Anderson DH, Johnson LV, et al. A common haplotype in the complement regulatory gene factor H (HF1/CFH) predisposes individuals to age-related macular degeneration. Proc Natl Acad Sci USA. 2005; 102:7227–7232. [PubMed: 15870199]
42. Haines JL, Hauser MA, Schmidt S, et al. Complement factor H variant increases the risk of age-related macular degeneration. Science. 2005; 308:419–421. [PubMed: 15761120]
43. Johnson PT, Betts KE, Radeke MJ, Hageman GS, Anderson DH, Johnson LV. Individuals homozygous for the age-related macular degeneration risk-conferring variant of complement factor H have elevated levels of CRP in the choroid. Proc Natl Acad Sci U S A. 2006; 103:17456–17461. [PubMed: 17079491]
44. Rogers J, Cooper NR, Webster S, et al. Complement activation by beta amyloid in Alzheimer disease. Proc Nat Acad Sci U S A. 1992; 89:10016–10020.
45. Heneka MT, O'Banion MK. Inflammatory processes in Alzheimer's disease. J Neuroimmunol. 2007; 184:69–91. [PubMed: 17222916]
46. Johnson PT, Brown MN, Pulliam BC, Anderson DH, Johnson LV. Synaptic pathology, altered gene expression, and degeneration in photoreceptors impacted by drusen. Invest Ophthalmol Vis Sci. 2005; 46:4788–4795. [PubMed: 16303980]
47. Hageman GS, Luthert PJ, Victor Chong NH, Johnson LV, Anderson DH, Mullins RF. An integrated hypothesis that considers drusen as biomarkers of immune-mediated processes at the RPE-Bruch's membrane interface in aging and age-related macular degeneration. Prog Retin Eye Res. 2001; 20:705–732. [PubMed: 11587915]
48. Crabb JW, Miyagi M, Gu X, et al. Drusen proteome analysis: an approach to the etiology of age-related macular degeneration. Proc Natl Acad Sci U S A. 2002; 99:14682–14687. [PubMed: 12391305]
49. Luibl V, Isas JM, Kayed R, Glabe CG, Langen R, Chen J. Drusen deposits associated with aging and age-related macular degeneration contain nonfibrillar amyloid oligomers. J Clin Invest. 2006; 116:378–385. [PubMed: 16453022]
50. Ding JD, Lin J, Mace BE, Herrmann R, Sullivan P, Bowes Rickman C. Targeting age-related macular degeneration with Alzheimer's disease based immunotherapies: anti-amyloid-beta antibody attenuates pathologies in an age-related macular degeneration mouse model. Vision Res. 2008; 48(3):339–345. [PubMed: 17888483]
51. Murisier F, Guichard S, Beermann F. Distinct distal regulatory elements control tyrosinase expression in melanocytes and the retinal pigment epithelium. Dev Biol. 2007; 303:838–847. [PubMed: 17196956]
52. Gupta N, Fong J, Ang LC, Yucel YH. Retinal tau pathology in human glaucomas. Can J Ophthalmol. 2008; 43(1):53–60. [PubMed: 18219347]

53. McKinnon SJ, Lehman DM, Kerrigan-Baumrind LA, et al. Caspase activation and amyloid precursor protein cleavage in rat ocular hypertension. Invest Ophthalmol Vis Sci. 2002; 43(4): 1077–87. [PubMed: 11923249]

54. McKinnon SJ. Glaucoma: Ocular Alzheimer's disease. Front Biosci. 2003; 8:1140–56.

55. Goldblum D, Kipfer-Kauer A, Sarra GM, Wolf S, Frueb BE. Distribution of amyloid precursor protein and amyloid-B immunoreactivity in DBA/2J glaucomatous mouse retinas. Invest Ophthalmol Vis Sci. 2007; 48(11):5085–5090. [PubMed: 17962460]

56. Guo L, Salt TE, Luong V, et al. Targeting amyloid-β in glaucoma treatment. Proc Natl Acad Sci U S A. 2007; 104:13444–13449. [PubMed: 17684098]

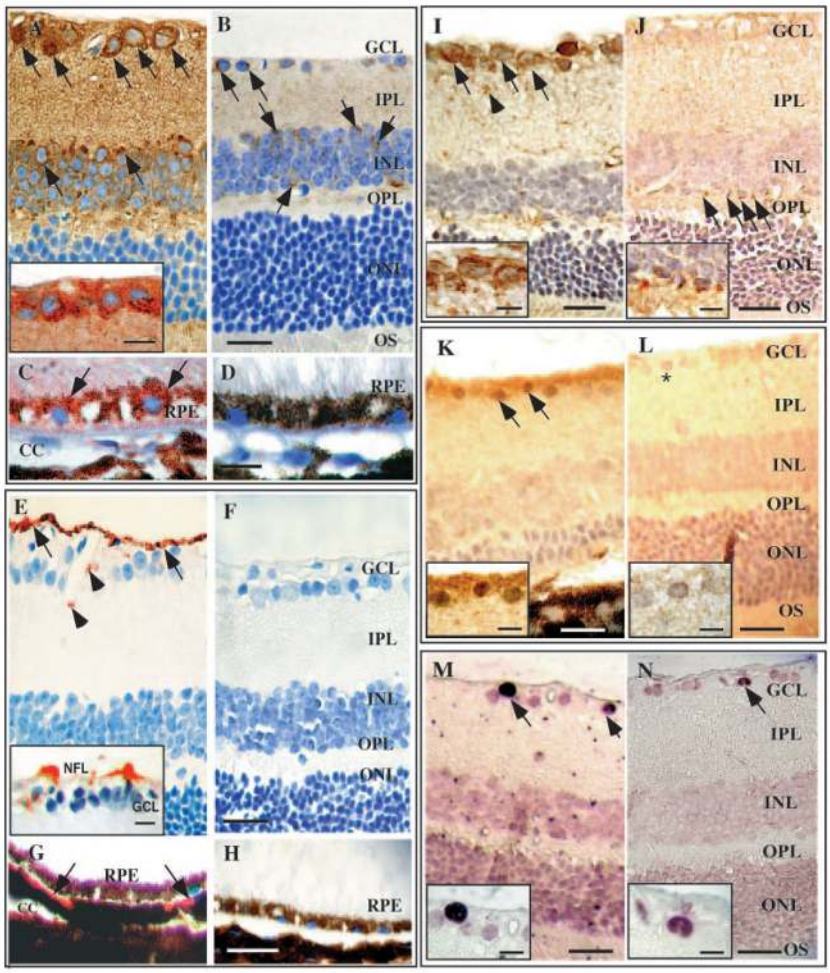

Figure 1.

Immunoreactivity for APP in (**A**, **C**) 27- and (**B**, **D**) 7.8-month-old animals from strain 1. (**A**) Strong DAB (*brown*) reaction was present in the cytoplasm of the cells in the GCL and INL (*arrows*), as well as in the neuropil of the IPL, OPL, and OS of the 27-month-old retina. *Inset*: another example of APP immunoreactivity in the cells of the GCL (AEC, *red*). Immunoreactivity was again confined to the cytoplasmic compartment of the large-caliber cells in the GCL. (**B**) Sparse DAB (*brown*) labeling in GCL and INL (*arrows*) of a 7.8-month-old retina. The neuropil exhibited background immunoreactivity only. Immunoreactiv-ity for APP (AEC, *red*) was (**C**) moderate in the cytoplasm of the RPE cells in the 27-month-old retina but was (**D**) at background levels in the RPE of the 7.8-month-old retina. Counterstain for nuclei: hematoxylin (*blue*). Immunoreactivity for amyloid-β in (**E**, **G**) 27- and (**F**, **H**) 7.8-month-old animals from strain 1. (**E**) Strong AEC (*red*) reaction was present, overlying the NFL (*arrows*) and in the retinal vasculature (*arrowheads*) of the 27-month-old animal. *Inset*: example of the amyloid-β deposits overlying the NFL of another 27-month-old animal. (**F**) A lack of amyloid-β immunoreactivity was found in the 7.8-month-old animal. The choroid vasculature demonstrated (**G**) moderate AEC-labeled deposits (*red*) of amyloid-β (*arrows*) in the 27-month-old animal, but (**H**) no amyloid-β immunoreactivity in the RPE and choroid of the 7.8-month-old animal. Counterstain for

nuclei: hematoxylin (*blue*). Immunoreactivity for F4/80 in (**I**) 27- and (**J**) 7.8-month-old animals from strain 1. (**I**) F4/80-immunoreactive profiles were labeled with DAB (*brown*). Intense staining was present in microglial profiles surrounding cells in the GCL (*arrows*, *inset*) of the 27-month-old animal, with large, ramified microglial profiles in the IPL (*arrowhead*). (**J**) There were F4/80-immunoreactive microglial profiles in the OPL of the 7.8-month-old animal, but no F4/80 immunoreactivity surrounding cells in the GCL. A few F4/80 microglial profiles were seen in the OPL (*arrows*, *inset*). Immunoreactivity for MCP-1 in (**K**) 27- and (**L**) 7.8-month-old animals from strain 1. (**K**) MCP-1 immunoreactivity (DAB, *brown*) was observed in the cytoplasmic compartment of cells in the GCL in the 27-month-old animal (*arrows*, *inset*), but (**L**) no MCP-1 immunoreactivity was observed in the GCL of the 7.8-month-old animal. *Inset*: high-power view of cells in GCL (✻). Labeling of the GCL of (**M**) 27- and (**N**) 7.8-month-old retinas in strain 1 showed TUNEL-AP–positive cells (*arrows*) in animals of both ages, but no TUNEL-AP–positive profiles in other layers of the retina. Scale bars: 10 μm (all *insets*; **C**, **D**); 20 μm (**A**, **B**, **E**–**M**).

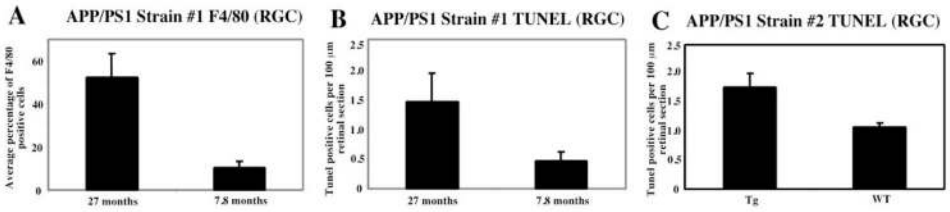

Figure 2.

(**A**) Percentage of cells in the GCL exhibiting F4/80 microglial profiles in 27- and 7.8-month-old animals (strain 1). The mean percentage of RGCs surrounded by F4/80-immunoreactive microglial profiles was 52.3% (SE ± 15.9%) in 27-month-old and 10.2% (SE ± 4.2%) in 7.8-month-old animals. (**B**) The mean number of TUNEL-AP–positive cells in the GCL per 100 μm of retina was greater in the 27-month-old retina (1.5 ± 0.5 SE) than in the 7.8-month-old retina (0.5 ± 0.2) in strain 1. (**C**) The mean number of TUNEL-AP–positive cells in the GCL per 100 μm of retina was greater in the 10.8-month-old transgenic animal (1.8 ± 0.2) compared with wild-type littermates (1.1 ± 0.1; strain 2). All comparisons reached significance ($P < 0.05$).

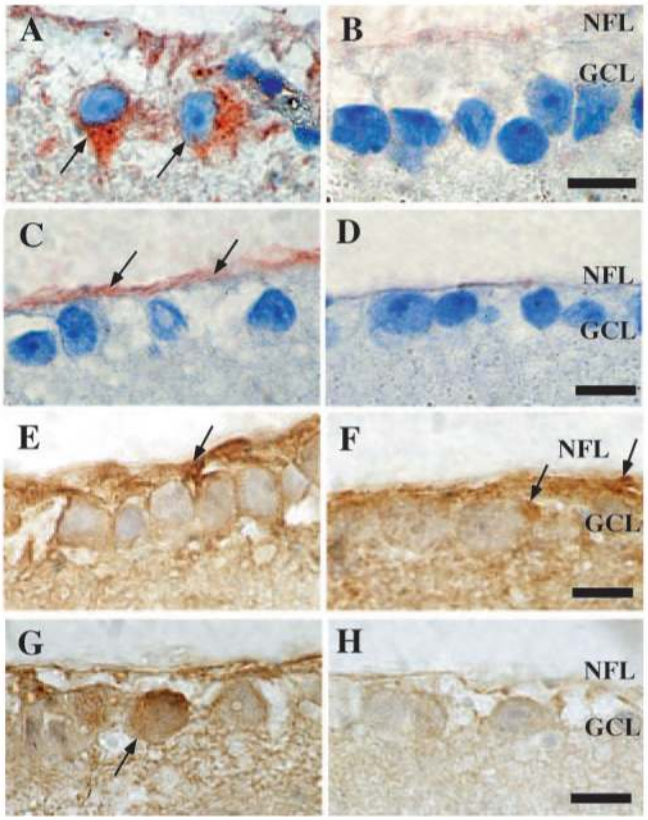

Figure 3.

(**A**, **B**) Immunoreactivity for APP in (**A**) 10.8-month-old transgenic and (**B**) wild-type littermate retinas from strain 2. (**A**) APP immunoreactive profiles, detected with AEC (*red*, *arrows*), showed intense staining of cytoplasmic compartments of cells in the GCL in (**A**) transgenic but not in (**B**) wild-type control retinas. (**C**, **D**) Immunoreactivity for amyloid-β in (**C**) 10.8-month-old transgenic and (**D**) wild-type littermate retinas from strain 2. (**C**) Amyloid-β deposits (AEC, *red*), were present overlying the NFL (*arrows*), whereas in (**D**) wild-type control retinas, labeling showed a lack of deposits on the NFL or surrounding cells in the GCL. (**E**, **F**) Immunoreactivity (DAB, brown) for F4/80 in (**E**) 10.8-month-old transgenic and (**F**) wild-type littermate retinas from strain 2 showed a similar quality of immunoreactivity surrounding cells in the GCL (**F**, *arrows*). (**G**, **H**) Immunoreactivity for MCP-1 (DAB, *brown*) in 10.8-month-old transgenic (**G**) and wild-type littermate (**H**) retinas from strain 2 showed staining of cells in the GCL of transgenic retinas (**G**, *arrows*), but no immunoreactivity in the wild-type control (**H**). Scale bars, 10 μm.

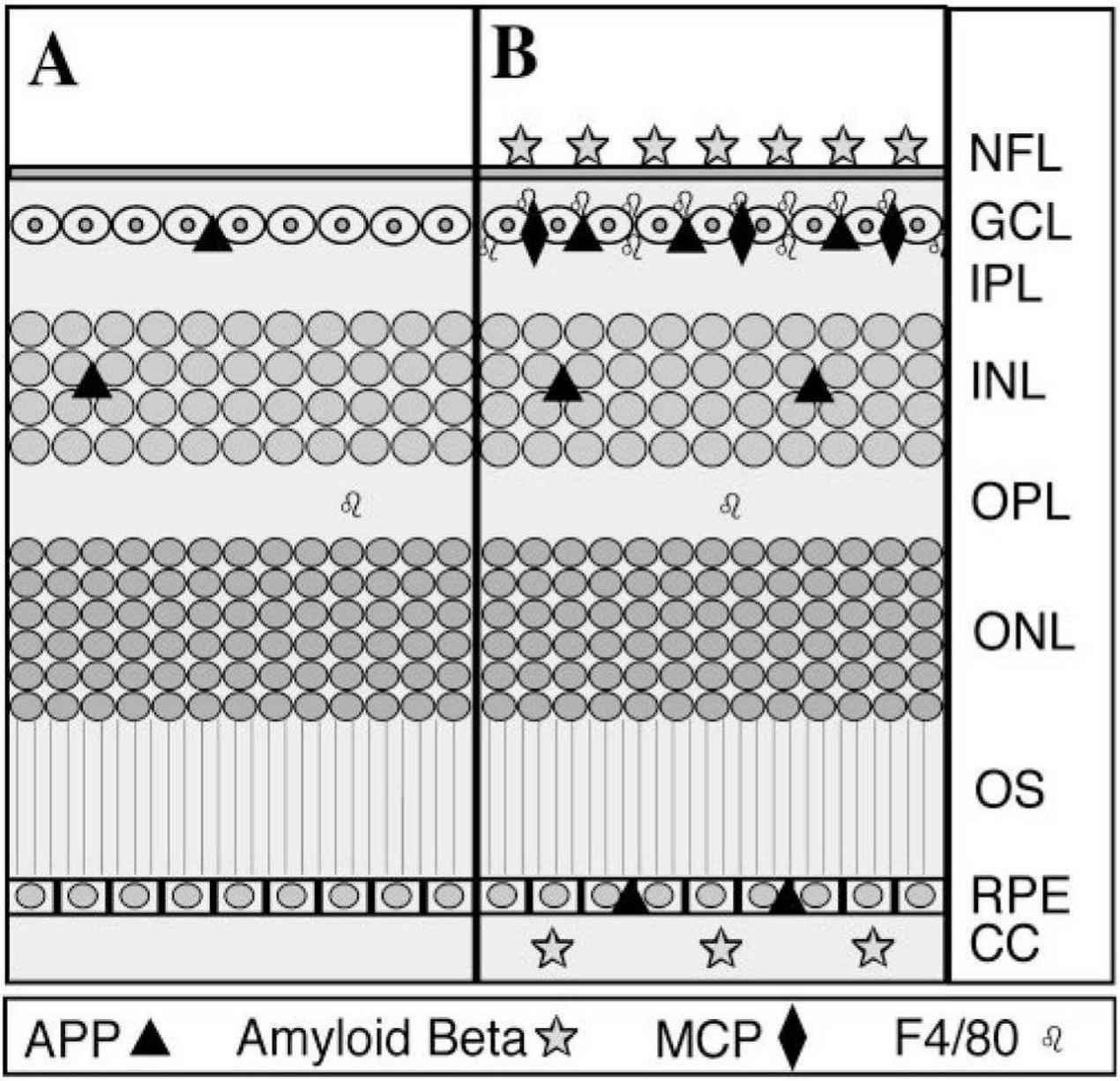

Figure 4.

(**A**, **B**) Summary diagram depicting age-dependent changes in APP, amyloid-β, microglia cells, and inflammatory cytokines (MCP-1) in the young (**A**) and old (**B**) APP/PS1 bitransgenic mice (strain 1). (**A**) Sparse immunoreactivity for APP in the cells of the GCL and in the INL was seen in the 7.8-month-old animals. An occasional F4/80-immunoreactive microglial profile was present in the OPL of the younger animals. (**B**) Robust immunoreactivity for APP was present in the cells of the GCL of the 27-month-old animal. The cells in the GCL also displayed robust cytoplasmic immunoreactivity for the cytokine MCP-1, and were heavily encrusted with F4/80-immunoreactive microglial profiles. The RPE cell of the 27-month-old animals displayed moderate APP immunoreactivity.

Concomitant deposits of amyloid-β were evident in the NFL and to a lesser extent, in the choroid of the 27-month-old animals of strain 1.

Table 1

Animal Data

Mouse Strain	ID	Age (mo)	APP	Amyloid-β	F4/80	MCP-1	TUNEL
Strain 1	21377	27	X	X	X	X	X
	21373	27	X	X	X	X	X
	27945	7.8	X	X	X	X	
	27946	7.8	X	X	X	X	X
	27947	7.8	X	X	X	X	X
Strain 2	WT A1	10.5			X	X	X
	WT A2	10.5	X	X			X
	WT C2	10.5	X	X	X		
	WT C4	10.5	X	X	X		
	WT C1	10.5	X	X			
	WT F2	10.5	X	X	X	X	X
	Tg B2	10.5	X	X	X		X
	Tg D1	10.5	X	X			X
	Tg D2	10.5	X		X	X	
	Tg D3	10.5	X	X			X
	Tg E3	10.5	X		X	X	
	Tg E4	10.5	X	X	X	X	X

Invest Ophthalmol Vis Sci. Author manuscript; available in PMC 2014 March 09.

TABLE 2

Antibodies

Primary Antibody	Secondary Antibody	Diluent	Chromogen	Primary Antibody Catalogue Number (Clone Number)
Anti-APP 1:5000; 30 min RT (Chemicon Temecula, CA)	Biotinylated horse anti-mouse, 1:100; 30 min RT (Vector Labs)	3% normal horse serum in 0.3% TX-100 and PB	AEC and DAB-GOD	MAB348 (22C11)
Anti Amyloid Beta 1:100; 3 h RT (Dako, Carpinteria, CA)	Biotinylated horse anti-mouse, 1:100; 30 min RT (Vector Labs)	3% normal horse serum in 0.3% TX-100 and PB	AEC	M0872 (6F/3D)
Anti F4/80 1:100; overnight at 4°C (Serotec, Raleigh, NC)	Biotinylated rabbit anti-rat, 1:100; 30 min RT (Vector Labs)	3% normal rabbit serum in 0.3% TX-100 and PB	AEC and DAB-GOD	MCAP497 (CI:A3-1)
Anti MCP-1 1:100; overnight at 4°C (R & D Systems, Minneapolis, MN)	Biotinylated rabbit anti-goat, 1:100; 30 min RT (Vector Labs)	3% normal rabbit serum in 0.3% TX-100 and PB	AEC and DAB-GOD	AF-479-NA (N/A, polyclonal)